S. Davis
Darwin G. Caldwell

Dept. of Electronic Engineering
University of Salford
Manchester M5 4WT, UK
s.davis@salford.ac.uk
d.g.caldwell@salford.ac.uk

Braid Effects on Contractile Range and Friction Modeling in Pneumatic Muscle Actuators

Abstract

Within braided pneumatic Muscle Actuators (pMA) the braid structure is vital to the actuator's performance, preventing over-inflation, converting radial expansion into axial contraction and setting limits for both dilation and contraction. This paper seeks to explore the nature of the contractile limit and the hysteresis observed by researchers during the actuation cycle.

Maximum actuator dilation occurs when adjacent braid strands are forced against one another. Within this work this is analyzed mathematically and it is shown that by halving the number of strands used to create the braided shell the actuator's contractile range can be increased by approximately 7%. This also results in a simultaneous peak contractile force increases of over 16%. These results are verified experimentally.

Hysteresis due to friction between braid strands during muscle operation is also explored. The paper will show how consideration of the deformation of the strands allows the contact area and therefore friction to be calculated without the need for experimentally obtained data as in previous research. A mathematical model is produced and verified experimentally.

KEY WORDS—actuators, braided pneumatic Muscle Actuators (pMA), McKibben muscles, friction, modeling

1. Introduction

Braided pneumatic Muscle Actuators (pMA) are a family of pneumatic drive that combine antagonistic characteristics of softness and compliance with powerful and accurate motion. There are a variety of techniques and materials used in the construction of braided pMA (also known as McKibben muscles) but to a very great extent the fundamental principles of the fabrication do not vary (Schulte 1962; Chou and Hannaford 1996; Tondu and Lopez 2000; Caldwell, Medrano-Cerda and Goodwin 1995; Klute and Hannaford 1998; Kingsley and Quinn 2002; Shadow Robot Company 2005; Paynter 1996; Inoue 1987; Festo Brochure; Bergemann, Lorenz and Thallemer 2002). In essence, there is a flexible inner cylindrical containment layer and an outer cylindrical braided woven layer with end caps to seal the cylinders. The inner layer has the function of enclosing and retaining the pressurized gas used to energize the muscle (i.e., prevent air escaping) while the outer braid which is in the form of a double helix forms a vital component that is the determining feature of many of the characteristics exhibited by the actuator. Attributes derived from the braid included the following:

(i) Acting as a restraining layer to prevent the over-inflation of the pressurized muscle, thereby preventing rupture.

(ii) Convertion of the largely radial expansion into axial contraction when the actuator is pressurized, thus generating the drive force needed to function as an actuator. It should be noted that the actuators can be used in an expansive mode (Walker et al. 2005) by compressing them beyond their contracted length before pressurization.

(iii) Setting of the limits of dilation and contraction. Modeling of the actuator has shown that a limit for contraction occurs at a braid angle of 54.7° (Schulte 1962). Limits for dilation (stretch) of the muscle are also set by the braid but in this instance this is determined by the nature of the weave.

(iv) Energy losses caused by friction between braid fibers causes a hysteresis component in the models of the actuators that reduces the contractile force and increase the control complexity. Previous work has shown that friction can be modeled experimentally (Chou and Hannaford 1996; Tondu and Lopez 2000) but where these experimental data are not available theoretical modeling is impossible using this technique.

The International Journal of Robotics Research
Vol. 25, No. 4, April 2006, pp. 359-369
DOI: 10.1177/0278364906063227

Pneumatic Muscle Actuators have a number of characteristics that may be of use in the field of robotics, such as high power-to-weight ratios, compliance and low cost of manufacture. This has resulted in them being used in a wide range of application. These include industrial robots (Inoue 1987), a nuclear waste manipulator (Caldwell et al. 1999), the walking robot Airbug (Berns et al. 2001) and a Microrobot Cricket (Birch et al. 2000).

In his early work Schulte demonstrated that pMAs could contract by up to 35% and developed a static model relating the force, supply pressure and contractile behavior (Schulte 1962). This model was typically accurate to within 10–20% for forces over the full operating range. Subsequently this model has been refined by several groups that have considered the effects of rounding of the terminal ends of the actuators (Tsagarakis and Caldwell 2000), finite thickness in the containment layers (Chou and Hannaford 1996), fatigue life (Klute and Hannaford 1998; Kingsley and Quinn 2002) and stretch of the braid fiber (Davis et al. 2003). Models have shown that the limit for contraction occurs at a braid angle of 54.7° (Schulte 1962). Limits for dilation (stretch) of the muscle are also set by the braid but in this instance are determined by the nature of the weave.

It has been observed by Chou and Hannaford (1996) and Tondu and Lopez (2000) that during operation there is a force/displacement hysteresis in the muscles caused by friction between the braid stands. Chou and Hannaford produced a model including an experimentally obtained force offset which was added to calculated forces during muscle contraction and subtracted during extension. Tondu and Lopez took this concept further by attempting to quantify the offset force by modeling the friction. Although the model produced was more accurate than that of Chou and Hannaford it still relied on a degree of experimental data.

Within this paper Section 2 develops a method of determining the minimum achievable braid angle for any given braid material. This is critical in determining the maximum dilated length of the actuator and thus its contractile range. Further, this analysis identifies a method for increasing both actuator contraction and peak force output through modification to the braid material. The actuator friction/hysteresis and its modeling are considered in Section 3, and a method is presented that enables theoretical actuator friction models to be developed without reference to experimental results. Section 4 has conclusions based on the work.

2. Braid Effects on the Limits of Contraction

The limit of contraction of pneumatic Muscle Actuators is typically 30–35% (Caldwell, Medrano-Cerda and Goodwin 1995) and is usually defined in terms of a change in the inter-braid angle (θ), Figure 1. At the fully contracted position the inter-braid angle is set by the energetics of the operation of the actuator at θ=54.7°. The maximum dilation (minimum braid angle) is limited by one of two factors, either by adjacent braid strands being forced against each other or by the diameter of the inner bladder being so large that it prevents full braid dilation. The proceeding analysis considers the case where the inner bladder has a diameter small enough to allow full braid dilation. This minimum braid angle can therefore vary depending on the weave pattern (typically a 2/2 Twill (Braidweaver 2005)), the fiber material and the diameter of the fiber. Typically the fully dilated braid angle is around 20° (Caldwell, Medrano-Cerda and Goodwin 1995).

The contractile range of the actuator is the difference between the length of the actuator at the minimum and maximum braid angles. As the maximum braid angle cannot be changed for this type of actuator it follows that the only way to increase the dynamic range is to permit the muscle to achieve a lower braid angle.

Previous studies of the minimum braid angle have been based on experimentally measured interweave angles; however, no theoretical basis or limit for the angle has been produced. To calculate the theoretical minimum angle consider a short section of braid around the muscle's circumference, Figure 1(a). This section can be "unrolled" to form the weave pattern shown in Figure 1(b), the axis is aligned along the length of the actuator. Letting each strand crossover point be known as a node, the distance between nodes will be G, the distance C is the circumference of the muscle and l is the inter-strand separation. To calculate l, consider the case where θ is 90°. At this point $C = 2 \cdot l \cdot N_c$ where N_C is the number of nodes in one circulation of the muscle's circumference. In Figure 1(b), $N_C = 3$.

When $\theta = 90°$ it is known that $C = \pi \cdot D_o$ where D_o is the theoretical muscle diameter at 90° and is found from (Schulte 1962)

$$D_O = \frac{b}{n \cdot \pi} \tag{1}$$

where b is the length of one strand used to form the braid and n is the number of times this strand spirals around the actuator.

Therefore

$$l = \frac{\pi \cdot D_o}{2 \cdot N_c} \tag{2}$$

and node separation G is given by

$$G = 2 \cdot l \cdot \sin\theta. \tag{3}$$

Figure 2 shows the structure of the braid if it is assumed that only one strand, of thickness W_B, follows each path. In reality each path is traced by several parallel strands but this does not effect the principle of the analysis.

It can be determined that

$$X = Y \cos\theta \Rightarrow Y = \frac{W_B}{2 \cdot \cos\theta}. \tag{4}$$

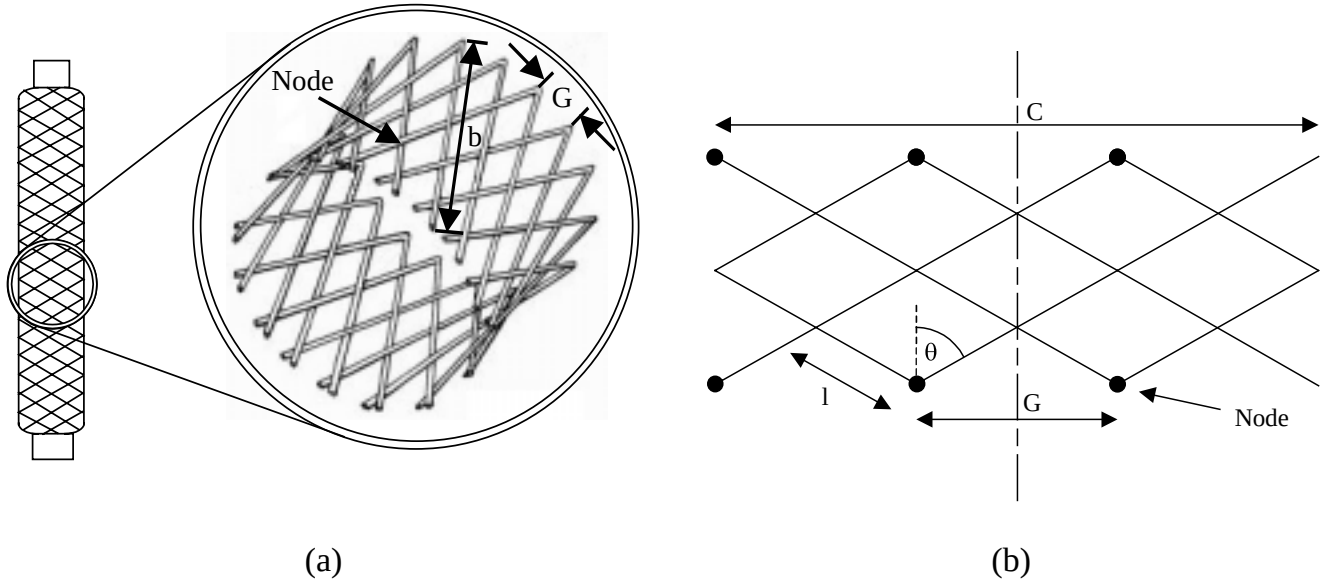

Fig. 1. Braid material (a) and unrolled (b).

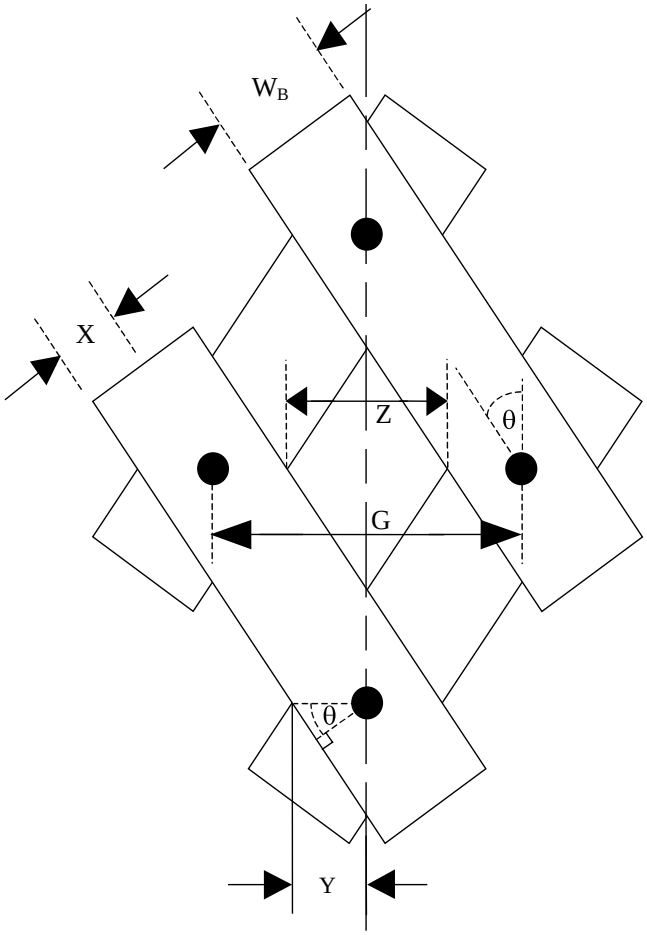

Fig. 2. Braid structure assuming single strands.

From Figure 2 it can be seen that the minimum braid angle $\theta_{\min}$ occurs when $G = 2 \cdot Y$ so from (2)–(4) the following equation for $\theta_{\min}$ can be produced:

$$\theta_{\min} = \frac{\sin^{-1}\left(\dfrac{2 \cdot W_B \cdot N_C}{\pi \cdot D_O}\right)}{2}. \tag{5}$$

It would be more useful if this equation was in terms of the known quantities D_s and N, the strand diameter and number of strands respectively. This can be achieved as follows:

$$W_B = D_S \cdot S \tag{6}$$

and

$$N_C = \frac{N}{2 \cdot S} \tag{7}$$

where D_s is the diameter of one strand, S is the number of parallel strands and N is the number of strands used to create the complete muscle. The equation for the minimum braid angle thus becomes

$$\theta_{\min} = \frac{\sin^{-1}\left(\dfrac{D_S \cdot N}{\pi \cdot D_O}\right)}{2}. \tag{8}$$

This angle will be a constant for any actuator irrespective of length, assuming that the values of D_s, S and N remain unchanged. However, in practical design applications it is more useful to know the maximum dilated length ($L_{\max}$) of an actuator. This can be calculated using the equation for actuator length introduced by Schulte (1962):

$$L_{\max} = b \cdot \cos\theta_{\min} \Rightarrow L_{\max} = b \cdot \cos\left[\sin^{-1}\left(\frac{D_S \cdot N}{\pi \cdot D_O}\right)\Big/2\right]. \quad (9)$$

2.1. Experimental Results

To verify the accuracy of the new braid angle model, tests were conducted on a sample of braid material, Figure 3(a), with the following properties:

$$D_o = 0.031 \text{ m} \quad D_s = 0.25 \text{ mm} \quad N = 240 \quad S = 3.$$

Each braid sample to be tested was suspended vertically with the upper section held securely in a clamp and the lower end loaded with a 3.2 kg mass which extends the braid to its maximum length. The minimum braid angle was then recorded; this was achieved by photographing the braid, enlarging the print and then measuring the angle. Measurements were take at ten points along the length of the braid (avoiding the extreme ends where the clamps prevented the minimum angle being achieved). The number of strands used to form the braid was then reduced (reducing N), by the removal of individual strands whilst D_o and D_s remained constant. The minimum braid angle was again recorded.

Figure 3 shows the braid at its fully extended length with the number of strands (N) being used to form the braid equal to 240 in Figure 3(a), 160 in Figure 3(b) and 120 in Figure 3(c). It can be seen that the minimum braid angle becomes smaller as the number of strands used to form the braid is reduced. Table 1 shows the mean measured minimum braid angles and the corresponding calculated values. It can be seen that the two values correspond closely with particularly good agreement for N equal to 120 and 240.

The dilated length of the actuator and therefore its stroke length is determined by the minimum braid angle and therefore this can be increased by making the angle as small as possible. For the braid tested here reducing the number of strands used to form the braid from 240 to 120 resulted in an increased actuator stroke length of approximately 7%. By studying eq. (8) it can be seen that as well as reducing the number of strands used to form the actuator the minimum braid angle can also be lowered by using strands with a smaller diameter.

The force generated by a muscle is dependent on braid angle with the largest force being generated at the smallest braid angle. It therefore follows that by reducing the minimum braid angle the peak actuator force can be increased. Equation (10) shows the ratio of the theoretical force (using the basic force equation (Schulte 1962)) for a braid angle of both 10° and 20°. It can be seen that the force at 10° is approximately 16% higher than that at 20° which represents an increase of peak static force of 16%:

$$\frac{F_{10}}{F_{20}} = \frac{\frac{\pi \cdot D_O^2 \cdot P}{4}(3\cos^2 10 - 1)}{\frac{\pi \cdot D_O^2 \cdot P}{4}(3\cos^2 20 - 1)} = 1.16. \quad (10)$$

It should be noted that during testing the samples only included the braid material; the internal rubber bladder was absent. Therefore, to achieve such a braid angle in a completed actuator the dilated diameter of the rubber bladder used should be less than the diameter of the braid at angle $\theta_{\min}$. If this is not the case the bladder will prevent the minimum braid angles being reached.

Table 1. Experimental Configurations

N	$\theta_{\min}$ Measured	Standard Deviation	$\theta_{\min}$ Calculated
240	18.9	0.57	19.0
160	13.7	1.16	12.1
120	9.6	0.97	9.0

2.2. Braid Area

When fewer strands are used in construction of the actuator this results in a more open structure, particularly as the muscle is pressurized. In its contracted state the muscle braid is now much more open and the gap between strands is larger than in a standard muscle. In some instances this may present a problem due to the internal bladder passing through the gaps and rupturing. It is therefore useful to know the relationship between the strands and the inter-fiber gap.

From Figure 1 it can be seen that the spacing between nodes G is

$$G = \frac{C}{N_c} \Rightarrow G = \frac{\pi \cdot D}{N_c} \quad (11)$$

where D is the diameter of the muscle and is given by $D_O \cdot \sin\theta$. Substituting this and (7) into (11) results in an equation for the node separation in known material properties:

$$G = \frac{2S \cdot \pi \cdot D_O \cdot \sin\theta}{N}. \quad (12)$$

As can be seen in Figure 2 the shape of the braid gaps is a rhombus of width Z:

$$Z = G - 2Y. \quad (13)$$

Substituting in eqs. (4), (6) and (12) gives

$$Z = \frac{2S \cdot \pi \cdot D_O \cdot \sin\theta}{N} - \frac{D_S \cdot S}{\cos\theta}. \quad (14)$$

The maximum area of the rhombus occurs at a braid angle of 45° and has an area given by $\frac{Z^2}{2}$, therefore

$$Area_{\text{Max}} = \frac{\left(\frac{2S \cdot \pi \cdot D_O \cdot \sin 45}{N} - \frac{D_S \cdot S}{\cos 45}\right)^2}{2}. \quad (15)$$

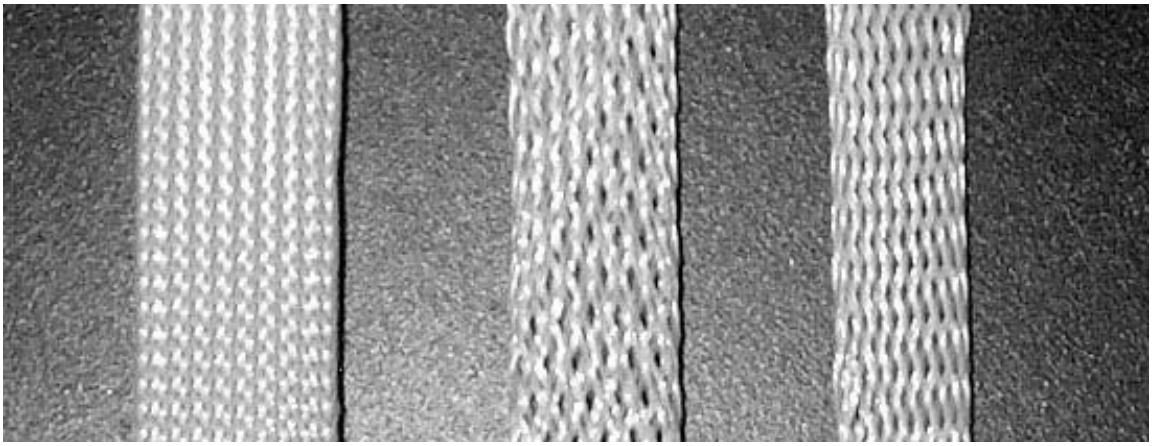

(a) (b) (c)

Fig. 3. Braid constructed with a range of strand numbers N.

For the braids tested the maximum gap area increased from 0.22 mm^2 for the braid consisting of 240 strands to 2.84 mm^2 when 120 strands were used. This represents a significant enlargement, greatly increasing the chances of the inner bladder passing through the gaps and rupturing. Anecdotal evidence suggests thinner bladder material is more likely to rupture and future work will study the nature of the bladder material and extend equation (15) to determine the point at which failure will occur.

2.3. Braid Failure

A second problem associated with removing braid strands is the reduction in overall braid strength. The radial force generated on the surface of the actuator, caused by the internal pressure, causes stretching of the braid strands (Davis et al. 2003). The force is equally distributed between each of the strands but as strands are removed so the force on each individual fiber increases and this will ultimately become so high that the structure fails. It is therefore essential for safety reasons that it be determined whether the braid used is capable of withstanding the forces to be applied to it.

To determine this the stress on an individual strand is analyzed. Due to the weave pattern the path of a single strand is a spiral along the length of the actuator circling it n times. Each circling n can be considered as a band around the circumference of the muscle. Hoop stress analysis can then be used to determine the increase in diameter of the band when a pressure is applied inside it (Ross 1987; Drucker 1967).

Hoop stress analysis is performed by considering the case where a cut is performed through the hoops at their widest point, as can be seen in Figure 4, and subsequently resolving the forces.

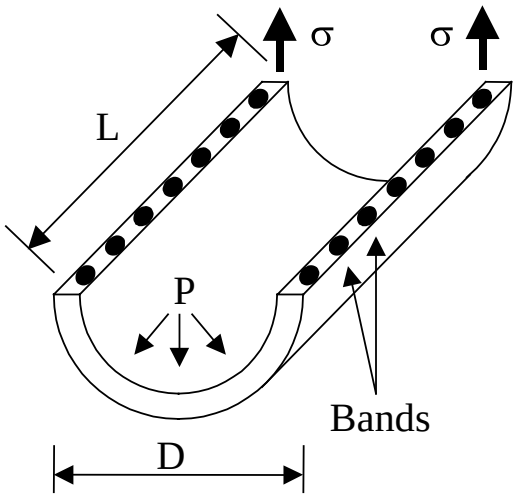

Fig. 4. Cut through actuator with strands considered as individual bands.

The total force in the vertical direction causing strand stretch equals $P \cdot D \cdot L$ therefore the force on each band is

$$\frac{P \cdot D \cdot L}{n \cdot N} \tag{16}$$

where n is the number of times each strand encircles the actuator and N is the total number of strands used to form the actuator. Therefore, the stress on each band is

$$\sigma = \frac{\dfrac{P \cdot D \cdot L}{n \cdot N}}{2 \cdot A_{\text{strand}}} = \frac{P \cdot D \cdot L}{2 \cdot n \cdot N \cdot A_{\text{strand}}} \tag{17}$$

where A_{strand} is the cross-sectional area of the strands in the same plane as the cut shown in Figure 4.

D is the actuator diameter given by (Chou and Hannaford 1996)

$$D = \frac{b \cdot \sin\theta}{n \cdot \pi} \tag{18}$$

and L is the actuator length given by (Chou and Hannaford 1996)

$$L = b \cdot \cos\theta. \tag{19}$$

It would be most useful to know the minimum number of braid strands necessary to prevent failure, therefore the equation can be rearranged thus:

$$N = \frac{P \cdot D_O^2 \cdot \pi \cdot \cos\theta \cdot \sin\theta}{2 \cdot \sigma \cdot A_{\text{strand}}}. \tag{20}$$

The ultimate tensile strength of the nylon material used to form the braid is 75×10^6 Pa (Brydson 1999) and the typical operating pressure of the actuators is 500 kPa. Therefore it can be calculated using (20) that the minimum number of braid strands that can be used to form an actuator with the material properties detailed earlier is 97.

This analysis allows for the construction of actuators with maximum contraction while ensuring safe operation is maintained.

3. Friction/Hysteresis

It has been observed by Chou and Hannaford (1996) and Tondu and Lopez (2000) that during operation there is a force/displacement hysteresis in the muscles. This is caused by friction between the braid stands. Tondu and Lopez (2000) also noted that although there is contact between the braid and the inner rubber liner this does not present a source of friction as the liner remains "rigidly locked" to the braid by the internal actuator pressure.

To account for the strand on strand friction in mathematical models Chou and Hannaford proposed adding a constant force offset to the calculated force during muscle contraction and subtracting it during extension (i.e., friction force always opposes the driving force). Tondu and Lopez (2000) took Chou and Hannaford's concept further by attempting to quantify the offset force by modeling the friction. However, the model produced is based on the basic static model which does not provide accurate force data (Schulte 1962; Chou and Hannaford 1996; Tsagarakis and Caldwell 2000; Davis et al. 2003). To overcome this, a parameter k is introduced which "tunes the slope of the considered static model" (Tondu and Lopez 2000). This ensures that the modeled data match the experimental values through the selection of an appropriate value of k. Although the model produced is more accurate than that of Chou and Hannaford, the method of producing it relies on experimental data.

In this section the approach taken by Tondu and Lopez is used to analyse the frictional effects present in the actuator and this is then combined with the more accurate static model described in Davis et al. (2003) which include stretching effects in the braid strands. This removes the need for the "tuning factor" k.

3.1. Braid Contact Area

When the strands used to make up the muscle braid move against one another they form a source of friction and this needs to be included in any mathematical model. The expression describing the static dry friction of the braid moving against itself is as follows (Tondu and Lopez 2000):

$$F_{\text{friction}} = f_s \cdot S_{\text{contact}} \cdot P \tag{21}$$

where F_{friction} is the resisting force caused by friction, f_s is the coefficient of friction (0.15–0.25 for a nylon on nylon contact (Plastics Design Library Staff 1995)) and S_{contact} is the contact area between the braid strands. Due to the weave of the braid, the contact area varies as the braid angle changes and so an expression for the contact area needs to be found. This is achieved by first considering just one braid crossover point as shown in Figure 5.

It can be seen that

$$\tan\theta = \frac{x}{y} \tag{22}$$

and

$$\sin\theta = \frac{W_B}{2y} \tag{23}$$

where θ is the braid angle as shown in Figure 5. The area of one contact polygon S_{one} is given by

$$S_{\text{one}} = 2 \cdot x \cdot y$$

therefore

$$S_{\text{one}} = \frac{W_B^2}{2 \cdot \cos\theta \cdot \sin\theta} \tag{24}$$

where, as before, W_B is the width of a strand assuming only a single strand follows each path. In reality several parallel strands are often used and therefore W_B is the total width of these parallel strands. The total contact area for the whole muscle is therefore

$$S_{\text{contact}} = \frac{N_{\text{contacts}} \cdot W_B^2}{2 \cdot \sin\theta \cdot \cos\theta} \tag{25}$$

where N_{contacts} is the total number of crossover points in the muscle.

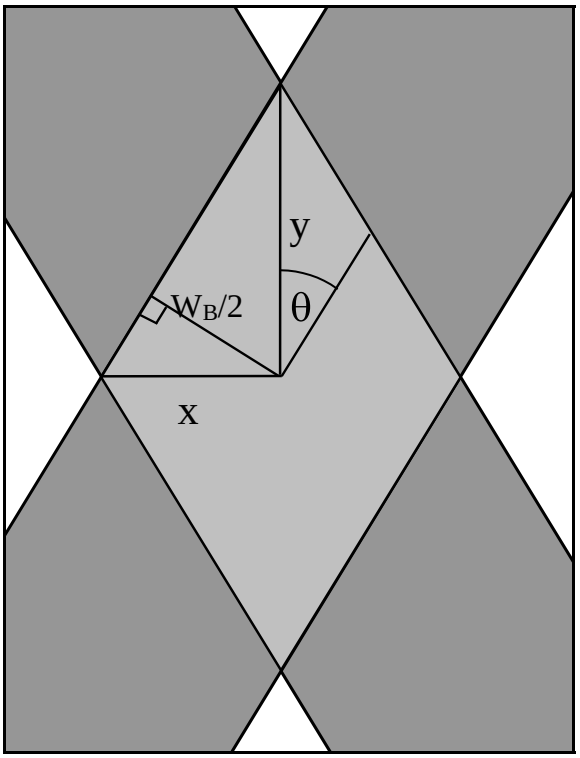

Fig. 5. One single braid crossover point.

The values for both W_B and N_{contacts} can both be obtained experimentally; however, this is difficult due to N_{contacts} being very high. However, if it is assumed that when the muscle is at its maximum dilation (minimum braid angle) there are no gaps between the crossover points, then the entire surface area of the muscle is made up of crossover points. Hence we can easily calculate the surface area of the muscle at its maximum length using eqs. (18) and (19) and $\theta_{\min}$ which can be calculated as described in Section 2.

Therefore at $\theta_{\min}$,

$$\textit{Surface area} = \pi \cdot D_{\min} \cdot L_{\max} = S_{\text{one}} \cdot N_{\text{contacts}}. \tag{26}$$

Substituting (22), (24) and (25) into (26) gives

$$N_{\text{contacts}} = \frac{2 \cdot b^2 \cdot \sin^2 \theta_{\min} \cos^2 \theta_{\min}}{n \cdot W_B^2} \tag{27}$$

so

$$S_{\text{contact}} = S_{\text{one}} \cdot N_{\text{contacts}} \tag{28}$$

and by combining (22), (27) and (28) we obtain an expression for the contact area of the whole muscle at any braid angle thus:

$$S_{\text{contact}} = \frac{b^2 \cdot \sin^2 \theta_{\min} \cdot \cos^2 \theta_{\min}}{n \cdot \sin \theta \cdot \cos \theta}. \tag{29}$$

Tondu and Lopez (2000) produced a similar expression; however, this format allows the variation in braid strand length described in Davis et al. (2003) to be included.

3.2. Frictional Effects

In the preceding analysis it has been assumed that the braid strands are of flat cross-section; however, in reality they are circular in cross-section and the basic friction equation (21) needs to be modified due to the circular nature of the braid strands. The contact surface calculated using (29) assumes that the strands are flat and this produces an overestimate of the contact area (Tondu and Lopez 2000). Therefore, a second constant S_{scale} is introduced which accounts for this by reducing the calculated contact area:

$$F_{\text{friction}} = f_s \cdot \frac{S_{\text{contact}}}{S_{\text{scale}}} \cdot P. \tag{30}$$

To produce a full model including friction the expression describing the frictional force needs to be combined with the static model thus (Tondu and Lopez 2000):

$$\begin{aligned} F_{SF} &= F_{\text{static}} - F_{\text{friction}} \text{ during contraction} \\ F_{SF} &= F_{\text{static}} + F_{\text{friction}} \text{ during dilation} \end{aligned} \tag{31}$$

where F_{SF} is the modeled output force including friction and F_{static} is the force calculated using the static force equation.

3.3. Experimental Results

To verify that the static model described in Davis et al. (2003) can be extended to include the effects of friction a test muscle with the following dimensions was used:

$b_{\min}$ = 0.65 m
n = 4.7
D_s = 0.00025 m
N = 240
f_s = 0.2 .

The muscle was pressurized to a predetermined test pressure and then a second, larger muscle was used to apply a force to the free end as shown in Figure 6. This allowed a range of differing forces to be applied to the test muscle. A load cell was placed at the point where the two muscles joined and a rotary potentiometer was used to measure the contraction of the test muscle. Although a hysteresis exists in both muscles the load cell was used to control the force applied to the test muscle and therefore the results are not affected by the hysteresis in the force muscle. As force was applied to the test muscle it increased in length and as a result its volume decreased. As the volume of air in the test muscle was constant this resulted in a pressure increase. To overcome this closed loop pressure control was used to maintain the pressure during testing.

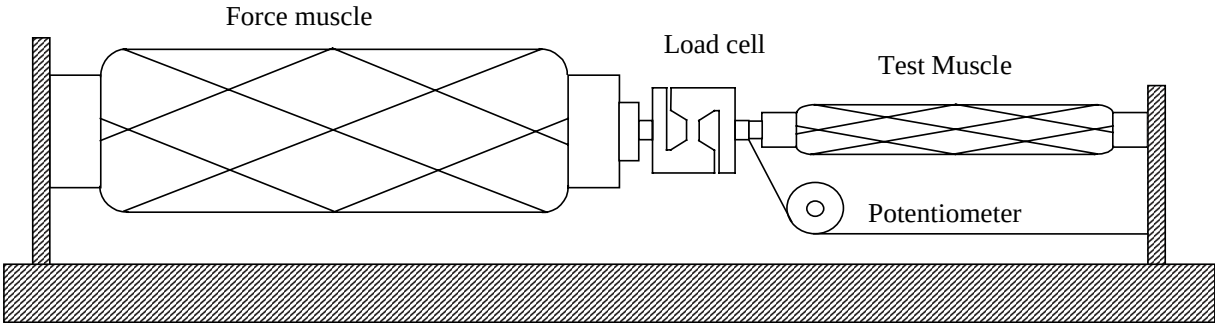

Fig. 6. Hysteresis test rig.

During testing an increasing force was applied to the test muscle and the contraction recorded. When the length of the muscle reached a predefined maximum the force was then gradually released. The experiment was repeated for a range of maximum muscle extensions to determine what effect this had on the size and shape of the hysteresis loop (Figure 7).

It can be seen that the width of the hysteresis loop, at each contraction length, remains constant despite varying the range of the test muscle's motion. This means that the frictional force F_{friction} calculated using (30) is valid for all ranges of motion at the pressure for which it is calculated.

To investigate the effect of pressure on the hysteresis the experiment was repeated at a range of test muscle pressures. The results are shown in Figure 8 and the modeled force/displacement relationship calculated using (31) is included. Suitable values of S_{scale} were selected from the experimental data and were found to be 20 at 200 kPa and 16 at 300 kPa.

This method of selecting an appropriate value of S_{scale} from the experimental results was used by Tondu and Lopez (2000) and a scaling factor of 13 was used in their work. The scaling factors used here and that used by Tondu and Lopez are in approximately the same range and the difference is likely to be due to the nature of the actuator materials used. Having to determine the scaling factor experimentally is not, however, desirable as the performance of any theoretical actuator cannot be calculated. It is more appropriate to calculate S_{scale} and this can be achieved by studying the structure of the weave used to form the braid and the points where friction occurs.

3.4. Strand Deformation

If the strands used to make up the braid were flat it would be simple to calculate the contact area between two touching strands. However, the cylindrical nature of the strands makes this more complex as the contact area is determined by the deformation of the material. If the cylinders were considered non-deformable as in Figure 9(a) the contact area would be negligible. In reality, however, all materials deform to some degree and therefore the contact area between the two strands, known as the Hertz contact area, is that shown in Figure 9(b).

The scaling factor S_{scale} can be calculated by determining the ratio of the work required to rotate two flat strands against each other and two cylindrical strands against each other. Calculation of the Hertz contact between two cylinders at any arbitrary angle θ is highly complex, requiring a finite-element-based approach. Therefore, for the purposes of this analysis the contact is considered as equivalent to the contact between two spheres, as can be seen in Figure 10.

The contact force between the two strands remains constant irrespective of the area of the contact. The distance that the two materials move against each other, however, does vary depending upon the contact area. Consider a circular contact area with radius a_c. If the upper sphere is rotated through one full revolution against the stationary lower sphere a point on the circumference of the contact area will travel a distance of $2\pi \mathrm{a}_c$. Now if the contact area is reduced so as to have a radius of $\mathrm{a}_c/2$ then a point on the circumference of this new contact area will only travel a distance of $\pi \mathrm{a}_c$, half that of the original point. Remembering that the contact force between the two spheres remains constant in both cases, the work required to rotate the sphere in the second instance must also be half that of the first. It therefore follows that the scaling factor will be

$$S_{\text{scale}} = \frac{a_c^{\text{flat}}}{a_c^{\text{sphere}}} \tag{32}$$

where a_c^{flat} is the contact radius assuming flat strands and is equal to $D_s/2$ and a_c^{sphere} is the contact radius assuming the contact to be between spheres.

The Hertz contact radius between two spheres is given by (Stolarski 1999)

$$a_c^{\text{sphere}} = 0.721 \left(F_{\text{comp}} \cdot Kd \cdot Ce\right)^{\frac{1}{3}} \tag{33}$$

where

$$Ce = \frac{2(1-\nu^2)}{E} \quad , F_{\text{comp}} = P \cdot D_s^2$$

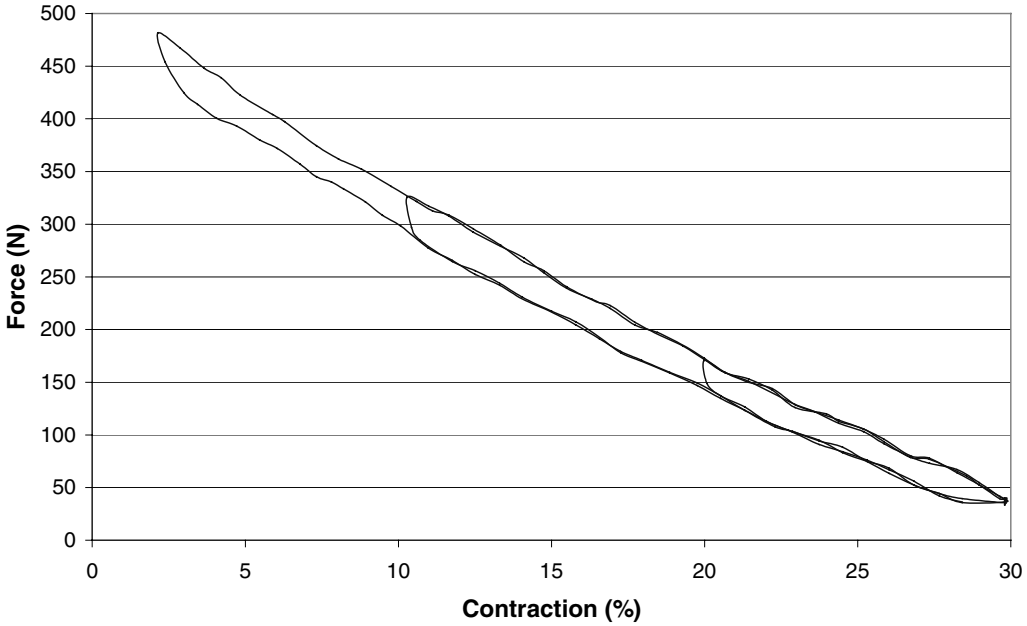

Fig. 7. Multiple loops with 200 kPa test pressure.

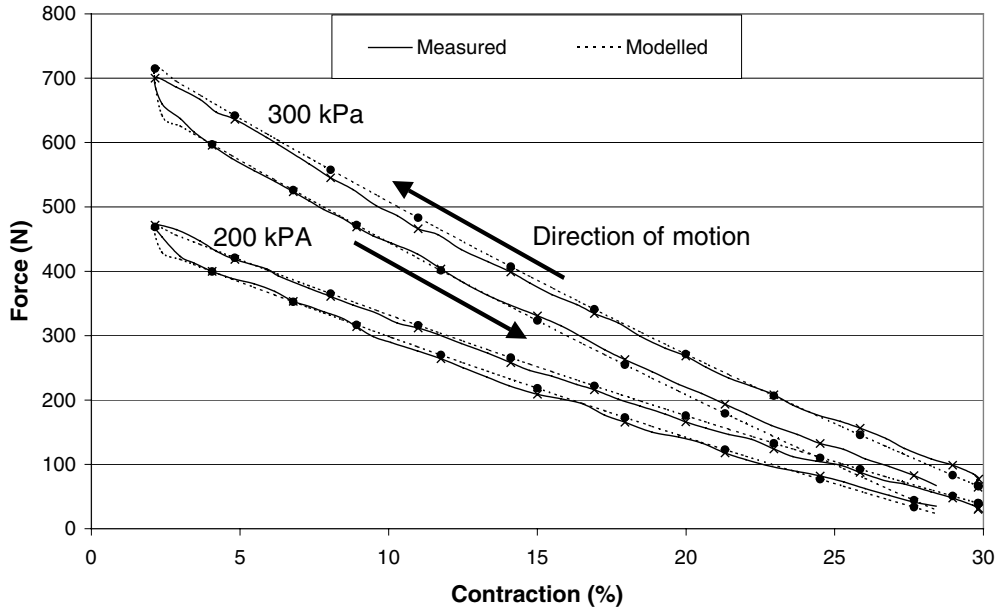

Fig. 8. Model and experimental results.

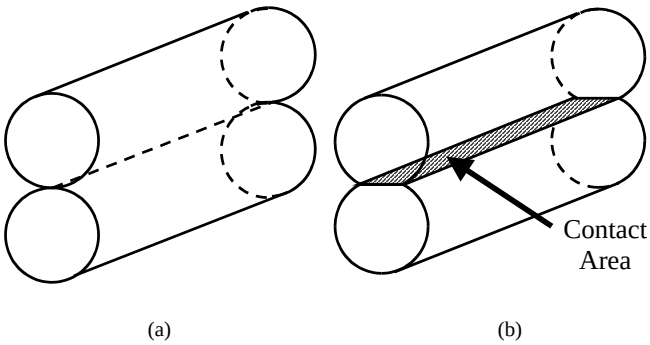

Fig. 9. Hertz contact between two parallel cylinders.

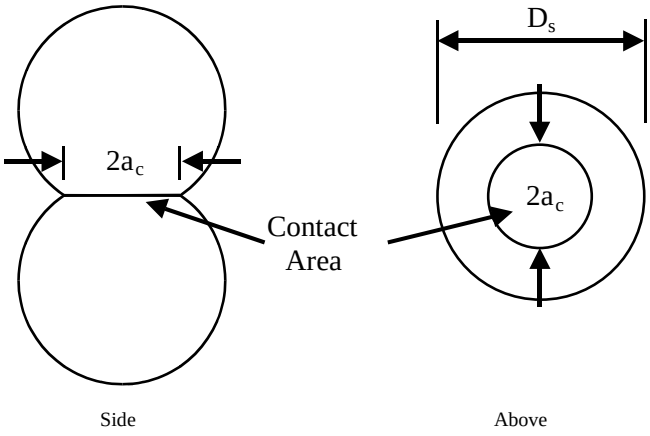

Fig. 10. Treating contact as that between two spheres.

and for equal radius spheres

$$Kd = \frac{D_s}{2}$$

with E being the Young's modulus, ν being the Poisson ratio of the strand material and F_{comp} being the force pushing the two strands together. Therefore the scaling factor is

$$S_{\text{scale}} = \frac{D_s/2}{0.721\left(F_{\text{comp}} \cdot \frac{D_s}{2} \cdot Ce\right)^{\frac{1}{3}}} = \frac{D_s}{1.442\left(F_{\text{comp}} \cdot \frac{D_s}{2} \cdot Ce\right)^{\frac{1}{3}}}. \quad (34)$$

For the test muscle

$E = 3 \times 10^9$ Pa (Brydson 1999)
$\nu = 0.4$ (Brydson 1999)
$D_s = 0.00025$ m

and this results in a value for S_{scale} of 18.1 for a 200 kPa drive pressure and 15.8 for a 300 kPa input. These values match the values obtained experimentally to better than 10%. The contact area increases as higher drive pressures are used as the material deformation is greater. This implies that the value of S_{scale} will not be a constant across all pressures and this is reflected in the experimentally obtained values of S_{scale}. Further evidence of this can be seen in the work of Tondu and Lopez (2000) where modeled force data using a scaling factor of 13 closely match the experimental data for a 400 kPa drive pressure, but as this pressure is reduced the accuracy of the model deteriorates.

The accuracy of the new model can also be verified using the experimental data presented by Tondu and Lopez (2000). Tondu and Lopez did not provide a value for the diameter of the braid strands used in their work but it seems reasonable to assume a similar material to that used in this work, and therefore a braid diameter of 0.25 mm was used during calculations. For a 400 kPa input pressure the scaling factor calculated using (34) is 14.3 which is within ≈10% of the experimentally obtained value of 13 of Tondu and Lopez. The difference is likely to be due to assumed strand diameter and the fact that the scaling factor of 13 was chosen to cover all operating pressures.

4. Conclusion

This paper has analyzed the structure of braided pneumatic Muscle Actuators and it has been shown that the minimum braid angle of the actuator can be calculated from the material properties of the actuator. This information is useful as the angle determines the dilated length and therefore the maximum stroke length of the actuator. The analysis has shown that by simply halving the number of strands used to create the braided shell of the actuator the minimum braid angle can be reduced by 50% (from 19° to 9°) and this results in an increase in actuator contraction of approximately 7% and an increase in peak contractile force of 16%. This result has also been proven experimentally.

As the number of fibers used to construct the braid is reduced the ability to contain the internal pressure decreases, ultimately leading to failure. Mathematical analysis has been used to determine the point at which this failure will occur. Further, reducing the number of fibers results in a more open braid structure, meaning the inner liner may pass through the braid and rupture. Further analysis of this will form future work.

It is well known that there is a force/displacement hysteresis in the actuators and whilst some work has considered this effect the resulting methods rely on data obtained experimentally from the actuator being modeled. This paper has presented a method allowing theoretical modeling (and experimental verification) of any generic actuator through analysis of strand contacts. Due to the cylindrical nature of the strands, calculation of the contact area is complex, and for

this reason past analysis has assumed flat strands and used a scaling factor to account for the circular cross-section of the strands. The scaling factor has usually been determined experimentally; however, this work has presented a mathematical method of determining the scaling factor using analysis of the Hertz contact between the strands and this has been verified against experimental data. It has been shown that the scaling factor is a pressure-dependant variable, not a constant as previously assumed.

References

Bergemann, D., Lorenz, B. and Thallemer, A. 2002. Actuating means. *US Patent* 6,349,746.

Berns, K., Albiez, J., Kepplin, V. and Hillenbrand, C. 2001. Airbug—insect-like machine actuated by fluidic muscle. *CLAWAR 2001*, Karlsruhe, Germany, pp. 237–244.

Birch, M. C., Quinn, R. D., Hahm, G., Phillips, S. M., Drennan, B., Fife, A., Verma, H. and Beer, R. D. 2000. Design of a cricket microrobot. *International Conference on Robotics and Automation*, San Francisco.

Braidweaver. 2005. www.braidweaver.com

Brydson, J. 1999. *Plastics Materials.* 7th Edition. Elsevier, Amsterdam.

Caldwell, D. G., Medrano-Cerda, G. A. and Goodwin, M. J. 1995. Control of pneumatic muscle actuators. *IEEE Control Systems Journal* 15(1):40–48.

Caldwell, D. G., Tsagarakis, N., Medrano-Cerda, G. A., Schofield, J. and Brown, S. 1999. Development of a pneumatic muscle actuator driven manipulator rig for nuclear waste retrieval operations. *International Conference on Robotics and Automation.* Detroit, IL.

Chou, P. and Hannaford, B. 1996. Measurement and modeling of McKibben pneumatic artificial muscles. *IEEE Transactions On Robotics and Automation* 12(1).

Davis, S., Tsagarakis, N., Canderle, J. and Caldwell, D. G. 2003. Enhanced modeling and performance in braided pneumatic muscle actuators. *International Journal of Robotics Research* 22(3).

De Haven, H., 1949. Tensioning device for producing a linear pull. *US Patent* 2,483,088.

Drucker, D. C. 1967. *Introduction to Mechanics of Deformable Solids.* McGraw-Hill, New York.

Festo Brochure. *Fluidic Muscle MAS*. Festo.

Inoue, K. 1987. Rubbertuators and applications for robots. *4th International Symposium On Robotics Research*, Santa Cruz, CA, pp. 57–64.

Kingsley, D. A. and Quinn, R.D. 2002. Fatigue life and frequency response of braided pneumatic actuators. *IEEE Robotics and Automation Conference.* Washington, DC, May 2002.

Klute, G. K. and Hannaford, B. 1998. Fatigue characteristics of McKibben artificial muscle actuators. *International Conference on Intelligent Robots and Systems Conference.* Victoria, Canada.

Paynter, H. M. 1996. Thermodynamic treatment of tug-&-twist technology: Part 1. Thermodynamic tugger design. *Japan/USA Symposium on Flexible Automation.* Boston, MA.

Pierce, R. C. 1936. Expansible cover. *US Patent* 2,041,950.

Plastics Design Library Staff. 1995. *Fatigue and Tribological Properties of Plastics and Elastomers*. William Andrew Publishing, Norwich, NY.

Ross, C. T. F. 1987. *Applied Stress Analysis*. Ellis Horwood, New York.

Schulte, R. A. 1962. The characteristics of the McKibben artificial muscle. *The Application of External Power in Prosthetics and Orthetics*, Publ. 874, Nas-RC, pp. 94–115.

Shadow Robot Company. 2005. www.shadow.org.uk

Stolarski, T. A. 1999. *Tribology in Machine Design*. Elsevier, Amsterdam.

Tondu, B. and Lopez, P. 2000. Modeling and control of McKibben artificial muscle robot actuators. *IEEE Control Systems Magazine.* April.

Tsagarakis, N. and Caldwell, D. G. 2000. Improved modeling and assessment of pneumatic muscle actuators. *ICRA 2000*, San Francisco.

Walker, I. D., Dawson, D., Flash, T., Grasso, F., Hanlon, R., Hochner, B., Kier, W. M., Pagano, C., Rahn, C. D. and Zhang, Q. 2005. *Continuum Robot Arms Inspired by Cephalopods. 2005 SPIE Conference on Unmanned Ground Vehicle Technology IV, Orlando, FL.*